

Holographic dark energy in a universe with spatial curvature and massive neutrinos: a full Markov Chain Monte Carlo exploration

Yun-He Li,^{1,*} Shuang Wang,^{1,2,†} Xiao-Dong Li,^{3,4,‡} and Xin Zhang^{§1,5,¶}

¹*Department of Physics, College of Sciences,
Northeastern University, Shenyang 110004, China*

²*Homer L. Dodge Department of Physics & Astronomy,
Univ. of Oklahoma, 440 W Brooks St., Norman, OK 73019, U.S.A.*

³*Institute of Theoretical Physics, Chinese Academy of Sciences, Beijing 100190, China*

⁴*Kavli Institute for Theoretical Physics China,
Chinese Academy of Sciences, Beijing 100190, China*

⁵*Center for High Energy Physics, Peking University, Beijing 100080, China*

In this paper, we report the results of constraining the holographic dark energy model with spatial curvature and massive neutrinos, based on a Markov Chain Monte Carlo global fit technique. The cosmic observational data include the full WMAP 7-yr temperature and polarization data, the type Ia supernova data from Union2.1 sample, the baryon acoustic oscillation data from SDSS DR7 and WiggleZ Dark Energy Survey, and the latest measurements of H_0 from HST. To deal with the perturbations of dark energy, we adopt the parameterized post-Friedmann method. We find that, for the simplest holographic dark energy model without spatial curvature and massive neutrinos, the phenomenological parameter $c < 1$ at more than 4σ confidence level. The inclusion of spatial curvature enlarges the error bars and leads to $c < 1$ only in about 2.5σ range; in contrast, the inclusion of massive neutrinos does not have significant influence on c . We also find that, for the holographic dark energy model with spatial curvature but without massive neutrinos, the 3σ error bars of the current fractional curvature density Ω_{k0} are still in order of 10^{-2} ; for the model with massive neutrinos but without spatial curvature, the 2σ upper bound of the total mass of neutrinos is $\sum m_\nu < 0.48$ eV. Moreover, there exists clear degeneracy between spatial curvature and massive neutrinos in the holographic dark energy model, which enlarges the upper bound of $\sum m_\nu$ by more than 2 times. In addition, we demonstrate that, making use of the full WMAP data can give better constraints on the holographic dark energy model, compared with the case using the WMAP “distance priors”.

[§] Corresponding author

*Electronic address: lyh19881206@126.com

†Electronic address: swang@mail.ustc.edu.cn

‡Electronic address: renzhe@mail.ustc.edu.cn

¶Electronic address: zhangxin@mail.neu.edu.cn

I. INTRODUCTION

Observations of type Ia supernovae (SNIa) [1], cosmic microwave background (CMB) [2] and large scale structure (LSS) [3] all indicate that the universe is undergoing an accelerating expansion. This implies the existence of a mysterious component, called dark energy [4], which has negative pressure and takes the largest proportion of the total density in the present universe. In the past fifteen years, lots of efforts [5–13] have been made to understand dark energy, yet we still know little about its nature.

In this paper we focus on the holographic dark energy model, which is a quantum gravity approach to the dark energy problem [14]. In this model, the vacuum energy is viewed as dark energy, and is related to the event horizon of the universe when we require that the zero-point energy of the system should not exceed the mass of a black hole with the same size [15]. In this way, we have the holographic dark energy density [16]

$$\rho_{de} = 3c^2 M_{Pl}^2 L^{-2}, \quad (1)$$

where c is a dimensionless phenomenological parameter which plays an important role in determining the properties of the holographic dark energy, M_{Pl} is the reduced Planck mass, and L is the IR cutoff length scale of the effective quantum field theory, which is taken to be the future event horizon of the universe, R_h , in the holographic model proposed by Li [16], defined as

$$R_h = a \int_t^\infty \frac{dt}{a} = a \int_a^\infty \frac{da}{Ha^2}. \quad (2)$$

The holographic dark energy model has been proven to be a competitive and promising dark energy candidate. It can theoretically explain the coincidence problem [16], and is proven to be perturbational stable [17]. Moreover, it is favored by the observational data [18]. For more studies on the holographic dark energy model, see, e.g., Refs. [19–23].

It is fairly difficult to calculate the cosmological perturbations of dark energy in the holographic dark energy model, because there is a non-local effect making the calculation of perturbations extremely hard to treat. Thus, in the past, for the CMB observations, only the WMAP “distance priors” data were used to constrain the holographic dark energy model in order to avoid the inclusion of the perturbations of dark energy (see e.g. Refs. [24–28]). However, recently, it has been realized that, in order to make progress one should first ignore the non-local effect in the holographic dark energy model and directly calculate the perturbations of holographic dark energy as if it is a usual dynamical dark energy. Along this line, in a recent work [29], a global fitting analysis on the holographic dark energy model was performed. However, in Ref. [29] the treatment of the gravity instability problem concerning the phantom divide crossing is absent.

In this paper, we shall perform a global fit analysis on the holographic dark energy model with spatial curvature and massive neutrinos. As argued in Ref. [30], the numerical studies of dynamical dark energy should include the spatial curvature Ω_{k0} as a free parameter to be fitted alongside the equation-of-state parameter (EOS) w of dark energy. In addition, the total mass of neutrinos $\sum m_\nu$ is also tightly correlated with w [31]. So, in our work, based on a Markov Chain Monte Carlo (MCMC) global fit technique, we will consider spatial curvature and massive neutrinos in the holographic dark energy model, and will deeply analyze the influences of these two factors on the fitting results. For a dynamical dark energy model, one must be careful about the treatment of perturbations in dark energy when w crosses -1 . In this work, following the WMAP team, we use the ‘‘parameterized post-Friedmann’’ (PPF) approach [32] implemented in the CAMB code.

This paper is organized as follows. In Section II, we derive the basic equations for the holographic dark energy in a universe with spatial curvature and massive neutrinos. In Section III, we discuss the holographic dark energy in a background universe and also in a perturbed universe, and then we make a global fit analysis on the models. At last, some concluding remarks are given in Section IV. In this work, we assume today’s scale factor $a_0 = 1$, so the redshift z satisfies $z = a^{-1} - 1$; the subscript ‘‘0’’ always indicates the present value of the corresponding quantity, and the unit with $c = \hbar = 1$ is used.

II. HOLOGRAPHIC DARK ENERGY MODEL WITH SPATIAL CURVATURE AND MASSIVE NEUTRINOS

In this section, we derive the basic equations for the holographic dark energy model with spatial curvature and massive neutrinos. Then we briefly introduce the PPF description of dark energy perturbations.

A. Background evolution of holographic dark energy in a non-flat universe

In a spatially non-flat Friedmann-Robertson-Walker universe, the Friedmann equation can be written as

$$3M_{pl}^2 H^2 = \rho_k + \rho_{dm} + \rho_{de} + \rho_b + \rho_\nu + \rho_r, \quad (3)$$

where $\rho_k = -3M_{pl}^2 K/a^2$ is the effective energy density of the curvature component, ρ_{dm} , ρ_{de} , ρ_b , ρ_ν and ρ_r represent the energy density of dark matter, dark energy, baryon, massive neutrinos and radiation, respectively. Notice that we adopt the approximate method used in the five-year analysis of WMAP [33]: dividing neutrino component into the relativistic neutrinos and the massive neutrinos, and including the relativistic neutrinos into radiation component. For convenience, we define the fractional energy densities of the

various components, $\Omega_i = \rho_i/(3M_{pl}^2 H^2)$. It is clear that

$$\Omega_k + \Omega_{dm} + \Omega_{de} + \Omega_b + \Omega_\nu + \Omega_r = 1. \quad (4)$$

In addition, the energy conservation equations for the various components are in the form

$$\dot{\rho}_i + 3H(1 + w_i)\rho_i = 0, \quad (5)$$

where $w_{1,2,3} = 0$ for dark matter, baryons and massive neutrinos, $w_4 = 1/3$ for relativistic components, $w_5 = -1/3$ for curvature and $w_6 = p_{de}/\rho_{de}$ for dark energy. Note that, in this paper, a over dot always denotes the derivative with respect to the cosmic time t . Combining Eqs. (4) and (5) gives

$$p_{de} = -\frac{2}{3}\frac{\dot{H}}{H^2}\rho_c - \rho_c - \frac{1}{3}\rho_r + \frac{1}{3}\rho_k, \quad (6)$$

which together with energy conservation equation (5) for dark energy gives

$$2(\Omega_{de} - 1)\frac{\dot{H}}{H} + \dot{\Omega}_{de} + H(3\Omega_{de} - 3 + \Omega_k - \Omega_r) = 0. \quad (7)$$

In a non-flat universe, the IR cut-off length scale L takes the form

$$L = ar(t), \quad (8)$$

where

$$r(t) = \frac{1}{\sqrt{|K|}} \text{sinn}\left(\sqrt{|K|} \int_t^{+\infty} \frac{dt}{a}\right) = \frac{1}{\sqrt{|K|}} \text{sinn}\left(\sqrt{|K|} \int_{a(t)}^{+\infty} \frac{da}{Ha^2}\right),$$

with $\text{sinn}(x) = \sin(x)$, x , and $\sinh(x)$ for $K > 0$, $K = 0$, and $K < 0$, respectively. From the energy density of the holographic dark energy, we have

$$\Omega_{de} = \frac{c^2}{H^2 L^2}. \quad (9)$$

Substituting Eq. (8) into Eq. (9) and taking derivative of Eq. (9) with respect to t , one can get

$$\frac{\dot{\Omega}_{de}}{2\Omega_{de}} + H + \frac{\dot{H}}{H} = \sqrt{\frac{\Omega_{de}H^2}{c^2} - \frac{K}{a^2}}. \quad (10)$$

Combining Eq. (7) with Eq. (10), we finally obtain the following two equations governing the dynamical evolution of the holographic dark energy in a universe with spatial curvature and massive neutrinos,

$$\frac{1}{E(z)} \frac{dE(z)}{dz} = -\frac{\Omega_{de}}{1+z} \left(\frac{\Omega_k - \Omega_r - 3}{2\Omega_{de}} + \frac{1}{2} + \sqrt{\frac{\Omega_{de}}{c^2} + \Omega_k} \right), \quad (11)$$

$$\frac{d\Omega_{de}}{dz} = -\frac{2\Omega_{de}(1 - \Omega_{de})}{1+z} \left(\sqrt{\frac{\Omega_{de}}{c^2} + \Omega_k} + \frac{1}{2} - \frac{\Omega_k - \Omega_r}{2(1 - \Omega_{de})} \right), \quad (12)$$

where $E(z) \equiv H(z)/H_0$ is the dimensionless Hubble expansion rate, and

$$\Omega_k(z) = \frac{\Omega_{k0}(1+z)^2}{E(z)^2}, \quad \Omega_r(z) = \frac{\Omega_{r0}(1+z)^4}{E(z)^2}. \quad (13)$$

The initial conditions are $E(0) = 1$ and $\Omega_{de}(0) = 1 - \Omega_{k0} - \Omega_{dm0} - \Omega_{b0} - \Omega_{\nu0} - \Omega_{r0}$. Note also that $\Omega_{\nu0}$ can be expressed as [34]

$$\Omega_{\nu0} = \frac{\sum m_\nu}{94h^2 \text{eV}}, \quad (14)$$

where h is the reduced Hubble constant, and $\sum m_\nu$ is the sum of neutrino masses. In addition, the value of Ω_{r0} is determined by the WMAP 7-yr observations [34]

$$\Omega_{r0} = 2.469 \times 10^{-5} h^{-2} (1 + 0.2271 N_{eff}), \quad (15)$$

where $N_{eff} = 3.04$ is the effective number of neutrino species. Thus, Eqs. (11) and (12) can be solved numerically, and will be used in the data analysis procedure.

In this paper, we shall consider the following four cases: (a) the model of holographic dark energy without spatial curvature and massive neutrinos ($\Omega_{k0} = 0$ and $\sum m_\nu = 0$), denoted as HDE; (b) the model of holographic dark energy with spatial curvature but without massive neutrinos ($\Omega_{k0} \neq 0$ but $\sum m_\nu = 0$), denoted as KHDE; (c) the model of holographic dark energy with massive neutrinos but without spatial curvature ($\sum m_\nu \neq 0$ but $\Omega_{k0} = 0$), denoted as VHDE; (d) the model of holographic dark energy with spatial curvature and massive neutrinos ($\Omega_{k0} \neq 0$ and $\sum m_\nu \neq 0$), denoted as KVHDE.

B. PPF description for the perturbations of holographic dark energy

In this work we calculate the linear metric and matter density perturbations by using the formalism of Ma and Bertschinger [35]. Also, we are very careful about the treatment of the divergence problem [36] for the dark energy perturbations when w crosses -1 . Following the WMAP team, we deal with this issue by using the PPF code [32]. This code supports a time-dependent EOS w that is allowed to cross -1 multiple times [37] for the dark energy perturbations. Moreover, it has been widely used in the literature to deal with the perturbations of dark energy (see e.g. Ref. [38]).

Now, we shall first briefly review the PPF description of dark energy perturbations [32, 37]. The perturbations of dark energy can be described by the following four variables, density fluctuation $\delta\rho_{de}$, velocity v_{de} , pressure fluctuation δp_{de} , and anisotropic stress Π_{de} . The evolution equations of $\delta\rho_{de}$ and v_{de} are given by corresponding continuity and Navier-Stokes equations, and Π_{de} vanishes for linear perturbations. To complete the system, one needs to specify the relationship between δp_{de} and $\delta\rho_{de}$, which defines a sound

speed $c_s^2 = \delta p_{de}^{(rest)} / \delta \rho_{de}^{(rest)}$, where ‘‘rest’’ denotes the dark energy rest frame. In an arbitrary gauge, one can obtain

$$\delta p_{de} = c_s^2 \delta \rho_{de} + 3(1+w)\rho_{de} \left(c_s^2 - \frac{\dot{p}_{de}}{\dot{\rho}_{de}} \right) \frac{v_{de}}{k_H}, \quad (16)$$

where $k_H = k/aH$ with k the wave number in the Fourier space. However, evidently, a gravity instability appears in the evolution of perturbations because of the divergence of $\dot{p}_{de}/\dot{\rho}_{de}$, when w crosses the phantom divide ($w = -1$).

The PPF description replaces this condition on the pressure perturbations with a direct relationship between the momentum density of the dark energy and that of other components on large scales, namely,

$$\lim_{k_H \ll 1} \frac{4\pi G}{H^2} (1+w)\rho_{de} \frac{v_{de} - v_T}{k_H} = -\frac{1}{3} c_K f_\zeta(a) k_H v_T, \quad (17)$$

where $c_K = 1 - 3K/k^2$, ‘‘ T ’’ denotes all other components excluding the dark energy, and $f_\zeta(a)$ is a function of time only. The PPF description can make an exact match at large scales to any given system with an arbitrary w by solving the full equations at $k_H \rightarrow 0$ and inferring $f_\zeta(a)$ for the evolution of all other finite k modes. However, it is sufficient for most purposes to simply take $f_\zeta = 0$ [32]. Note that once v_{de} is determined, δp_{de} follows by momentum conservation with no singularities encountered as w crosses the phantom divide.

Besides, PPF description of dark energy gives the density and momentum components of dark energy with a single joint dynamical variable Γ . Here we directly give these two relationships in the synchronous gauge,

$$\rho_{de} \delta_{de} = -3\rho_{de}(1+w) \frac{v_{de}}{k_H} - \frac{c_K k_H^2 H^2}{4\pi G} \Gamma, \quad (18)$$

$$\rho_{de}(1+w)v_{de} = \rho_{de}(1+w)v_T - \frac{k_H H^2}{4\pi G} \frac{1}{F} \left[S - \Gamma - \frac{\dot{\Gamma}}{H} + f_\zeta \frac{4\pi G(\rho_T + P_T)(v_T + k\alpha)}{k_H H^2} \right], \quad (19)$$

where

$$F = 1 + 3 \frac{4\pi G a^2}{k^2 c_K} (\rho_T + p_T),$$

and

$$S = -\frac{4\pi G}{H^2} \left[f_\zeta (\rho_T + p_T) - \rho_{de}(1+w) \right] \frac{(v_T + k\alpha)}{k_H}.$$

Here $\delta_{de} \equiv \delta \rho_{de} / \rho_{de}$ and $\alpha \equiv a(\dot{h} + 6\dot{\eta}) / 2k^2$ with h and η the metric perturbations in the synchronous gauge.

At last, to assure that the dark energy becomes smooth relative to the matter inside a transition scale $c_s k_H = 1$ while exactly conserving energy and momentum locally, one takes

$$(1 + c_\Gamma^2 k_H^2) \left[\frac{\dot{\Gamma}}{H} + \Gamma + c_\Gamma^2 k_H^2 \Gamma \right] = S, \quad (20)$$

where the free parameter c_Γ gives the transition scale between the large scales and small scales in terms of the Hubble scale, whose value needs to be calibrated in practice. It is found that $c_\Gamma = 0.4c_s$ could match the evolution of scalar field models [32]. Note that the PPF approach doesn't define a sound speed c_s for dark energy, but its value may indirectly influence the perturbations of dark energy, since we adopt $c_\Gamma = 0.4c_s$. The possible influences of c_s on the amplitude of dark energy perturbations can be found in Refs. [39–45]. As long as c_s is close to 1, the dark energy does not cluster significantly on sub-horizon scales. Therefore, following the treatment in the CAMB and CMBFAST codes, in our analysis we set c_s to be 1.

For the details about the PPF approach, we refer the reader to Refs. [32, 37]. Note that the CAMB Einstein-Boltzmann package has been modified to include PPF [32] and a version for dark energy has been made publically available¹. In our calculations, the initial condition for the dynamical variable Γ of PPF is set to be zero and the adiabatic initial conditions are taken for other variables.

III. GLOBAL FIT ANALYSIS

In this section, we shall make a global fit analysis on the holographic dark energy models considered above. We modify the MCMC package ‘‘CosmoMC’’ [46] to do the numerical calculations. Our most general parameter space vector is:

$$\mathbf{P} \equiv (\omega_b, \omega_{dm}, \Theta, \tau, c, \Omega_{k0}, \sum m_\nu, n_s, A_s), \quad (21)$$

where $\omega_b \equiv \Omega_{b0}h^2$ and $\omega_{dm} \equiv \Omega_{dm0}h^2$, Θ is the ratio (multiplied by 100) of the sound horizon to the angular diameter distance at decoupling, τ is the optical depth to re-ionization, c is the phenomenological parameter of the holographic dark energy model, A_s and n_s are the amplitude and the spectral index of the primordial scalar perturbation power spectrum. For the pivot scale, we set $k_{s0} = 0.002\text{Mpc}^{-1}$ to be consistent with the WMAP team [34].

In the computation of the CMB anisotropy, we include the WMAP 7-yr temperature and polarization power spectra [34] with the routine for computing the likelihood supplied by the WMAP team [47]. For the SNIa, we make use of the recently released 580 SNIa data from the ‘‘Union2.1’’ sample [48], where the systematic errors of SNIa are included in our analysis. For the LSS information, we use the BAO data from the SDSS DR7 [49] and WiggleZ Dark Energy Survey [50]. In addition, we also use the latest Hubble space telescope (HST) measurement of the Hubble constant, $H_0 = 73.8 \pm 2.4 \text{ km s}^{-1} \text{ Mpc}^{-1}$ [51].

Before constraining the model parameter space, we study the effects of the phenomenological parameter c on the background evolution, CMB power spectrum, and structure growth, by setting different c and fixing

¹ <http://camb.info/ppf/> (PPF module for CAMB).

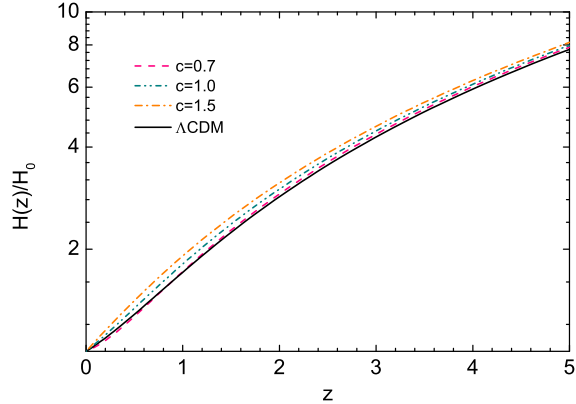


FIG. 1: The evolution of the dimensionless Hubble expansion rate $H(z)/H_0$ in the holographic dark energy model. As an example, we show the cases with $c = 0.7$, $c = 1.0$, and $c = 1.5$. For a comparison, the case in the Λ CDM model is also plotted. For the other model parameters, we adopt their best-fit values given by the WMAP 7-yr observations.

the other model parameters. For simplicity, in these examples we only consider the holographic dark energy model in a flat universe.

First, let us have a look at the background evolution. The parameter c in the holographic dark energy model plays a very significant role in determining the dynamical evolution of dark energy; for details see Ref. [18]. In order to see the influence of c on the dynamics of expansion of the universe, we plot the evolution of $H(z)/H_0$ for the holographic dark energy model in Fig. 1. We take the values of c to be 0.7, 1.0, and 1.5, as examples. We also plot the evolution of the Λ CDM model for a comparison in this figure. For the other model parameters, we adopt their best-fit values given by the WMAP 7-yr observations [34]. From this figure, we can see that different c values in the holographic model lead to distinctly different expansion histories. However, taking an appropriate value for c , such as $c = 0.7$, the holographic dark energy model will produce a nearly indistinguishable background expansion history with the Λ CDM model.

Next, we want to see the situations in a perturbed universe. The results of the CMB C_l^{TT} power spectrum in the holographic dark energy model are shown in Fig. 2. For comparison, we also plot the results of the XCDM models with different constant w . One can see that, for the holographic models with different c , the main difference appears at low ($l < 20$) multipole momentum parts which correspond to large scales. As seen in this figure, a smaller c will yield a smaller C_l^{TT} at low l . Besides, since the EOS of the holographic dark energy satisfies $w = -\frac{1}{3} - \frac{2\sqrt{\Omega_{de}}}{3c}$ [16], a smaller c will give a smaller w . So for the HDE model, a smaller w will lead to a smaller C_l^{TT} at low l . Similarly, for the XCDM model, a smaller w will also lead to a smaller C_l^{TT} at low l . Thus, the results of the HDE and XCDM models are consistent with each other. We also notice that, for the CMB temperature angular power spectrum, the holographic dark energy model

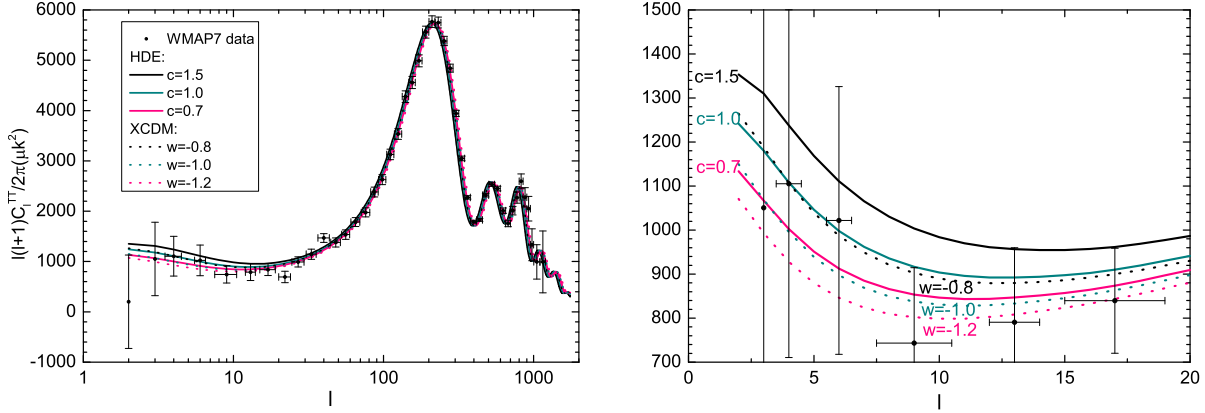


FIG. 2: The CMB C_l^{TT} power spectrum in the holographic dark energy model. The black dots with error bars denote the observed data with their corresponding uncertainties from WMAP 7-yr results. The solid lines denote the holographic dark energy models with different c , and the dotted lines denote the XCDM models with different w . For the other model parameters, we adopt their best-fit values given by the WMAP 7-yr observations.

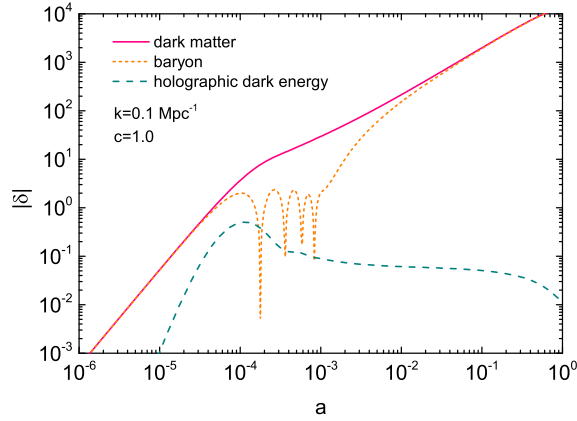


FIG. 3: Evolution of the density fields in the synchronous gauge for $k = 0.1 \text{ Mpc}^{-1}$ in the holographic dark energy model with $c = 1$. The pink solid line, orange short-dashed line, and cyan dashed line denote the density perturbations of dark matter, baryon, and holograph dark energy, respectively. For the other model parameters, we adopt their best-fit values given by the WMAP 7-yr observations.

with $c = 0.7$ can also produce a roughly same result with the Λ CDM model.

Figure 3 shows the evolution of the density perturbations for dark matter, baryon, and holographic dark energy, in the HDE model with $c = 1$ in the synchronous gauge. As a typical example, we only plot the $k = 0.1 \text{ Mpc}^{-1}$ case. The behavior of the density perturbations outside the horizon is strongly gauge-dependent. In the synchronous gauge, all the δ 's before horizon crossing grow. After horizon crossing, the perturbations come into causal contact and become nearly independent of the coordinate choices. For the cold dark matter, after the horizon crossing the fluctuations still monotonously grow. The mode with

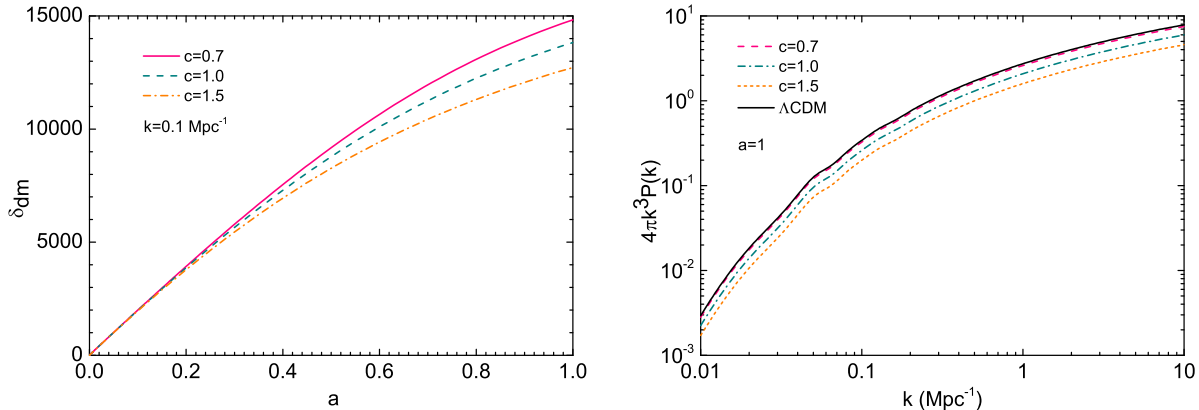


FIG. 4: Left panel: the evolution of the density perturbations of cold dark matter for $k = 0.1 \text{ Mpc}^{-1}$. Right panel: the matter power spectra at $z = 0$. The cases of $c = 0.7$, $c = 1.0$, and $c = 1.5$ in the holographic dark energy model are shown. For the other model parameters, we adopt their best-fit values given by the WMAP 7-yr observations.

$k = 0.1 \text{ Mpc}^{-1}$ enters the horizon before recombination, so the baryons together with the photons oscillate acoustically while they are coupled by Thomson scattering. The baryons decouple from the photons at the recombination and then fall very quickly into the potential wells formed around the cold dark matter, resulting in the rapid growth of δ_b , as seen in Fig. 3. For the holographic dark energy, we see clearly that after the horizon crossing, the fluctuations in dark energy decrease quickly. So, the dark energy does not cluster significantly on the sub-horizon size. During the expansion of the universe, δ_{de} is always smaller than δ_{dm} by several orders of magnitude, so the dark energy perturbations almost do not affect the evolution of cold dark matter perturbations. Hence, the impact of holographic dark energy on the evolution of dark matter perturbations is almost only from the background evolution. In the Λ CDM model, the cosmological constant does not produce fluctuations, so its impact on the evolution of dark matter density fluctuations is exactly from the background evolution.

In order to know more about the large-scale structure in the holographic dark energy model, we plot the evolution of dark matter density perturbations and matter power spectrum with different c values in Fig. 4. From the left panel of Fig. 4, we can directly see the impact of the value of c on the growth of structure. Again, we take the case of $k = 0.1 \text{ Mpc}^{-1}$ as an example. Once the accelerated expansion begins, the growth of linear perturbations effectively tends to end, since the Hubble damping time becomes shorter than the timescale for perturbation growth. For larger c and fixed present dark energy density Ω_{de0} , dark energy comes to dominate earlier, causing the growth of linear perturbations to end earlier; this explains the amplitude of perturbation with smaller c is larger at all redshifts until today. In the right panel of Fig. 4, we show the matter power spectra with different values of c at $z = 0$ in the holographic dark energy model. We

find that the impact of c on the small scales is slightly larger than that on the large scales. We also make a comparison with the Λ CDM model. It is found that the HDE model with $c = 0.7$ and the Λ CDM model produce the almost undistinguishable matter power spectra.

So far, we have deeply analyzed the holographic dark energy model in the aspects of background universe, CMB, and LSS. We find that the parameter c plays an important role in all these aspects. We also find that the HDE model with $c \simeq 0.7$ strongly degenerates with the Λ CDM model. In the following, we perform a global fit on the holographic dark energy models by using the full CMB data combined with the data of SNIa, BAO, and Hubble constant.

For the four holographic dark energy models considered, we run 16 independent chains with $\sim 20,000$ samples in each chain. The following priors to model parameters are adopted: $\omega_b \in [0.005, 0.1]$, $\omega_{dm} \in [0.01, 0.99]$, $\Theta \in [0.5, 10]$, $\tau \in [0.01, 0.8]$, $c \in [0.3, 1.5]$, $\Omega_{k0} \in [-1, 1]$, $n_s \in [0.5, 1.5]$, and $\log[10^{10} A_s] \in [2.7, 4]$. Furthermore, the hard coded prior on the cosmic age $10 \text{ Gyr} < t_0 < 20 \text{ Gyr}$ is also imposed and the parameter f_ν (the definition is the ratio between the current densities of massive neutrinos and cold dark matter) ranges from 0 to 1. We did not use the option MPI Check Limit Converge, but we find the chains converge at acceptable values. Values of $-\ln \mathcal{L}_{max}$ and convergence (the worst e -values [the variance(mean)/mean(variance) of 1/2 chains] $R - 1$) for the four models are listed in the Table I. Table I summarizes the fitting results, including the best-fit and $1-3\sigma$ values of the relevant cosmological parameters, as well as the 2σ upper bounds of $\sum m_\nu$, for the considered models. Moreover, we also list the maximal confidence levels for $c < 1$, in this table. In addition, in Figs. 5–7, we plot the 1D marginalized distributions of individual parameters,² as well as the 2D marginalized $1-3\sigma$ CL contours, for these models. Let us discuss them in detail in what follows.

The fitting results of the HDE model are shown in Fig. 5. We find that the values of c in $1-3\sigma$ regions are $c = 0.680^{+0.064+0.135+0.222}_{-0.066-0.119-0.159}$; note that the error bars are slightly smaller than those obtained by using the WMAP “distance priors” [28]. Moreover, we find that $c < 1$ at 4.2σ CL, which means that the future universe will be dominated by phantom energy and will end up with a “Big Rip” (cosmic doomsday) at more than 4σ CL. In Ref. [23] it has been demonstrated that $c < 1$ may lead to the ruin of the theoretical foundation—the effective quantum field theory—of the holographic dark energy scenario. To rescue the holographic scenario of dark energy, one may employ the braneworld cosmology and incorporate the extra-dimension effects into the holographic theory of dark energy. It has been found [23] that such a mend could erase the big-rip singularity and leads to a de Sitter finale for the holographic cosmos. In addition, if there

² We find that the 1D marginalized posteriors and mean likelihoods of c , $\sum m_\nu$, and Ω_{k0} are close to each other and have the same shapes, thus here we only show the marginalized posteriors.

TABLE I: Fitting results of the holographic dark energy models.

Parameters	HDE	KHDE	VHDE	KVHDE
$\Omega_{dm0}h^2$	$0.110^{+0.005+0.009+0.013}_{-0.002-0.006-0.010}$	$0.113^{+0.007+0.012+0.016}_{-0.002-0.007-0.012}$	$0.110^{+0.006+0.009+0.012}_{-0.002-0.005-0.009}$	$0.117^{+0.009+0.015+0.021}_{-0.004-0.009-0.016}$
$100\Omega_b h^2$	$2.259^{+0.061+0.115+0.159}_{-0.048-0.100-0.152}$	$2.246^{+0.063+0.121+0.159}_{-0.045-0.098-0.142}$	$2.272^{+0.044+0.096+0.144}_{-0.069-0.105-0.155}$	$2.256^{+0.028+0.097+0.146}_{-0.066-0.128-0.173}$
c	$0.680^{+0.064+0.135+0.222}_{-0.066-0.119-0.159}$	$0.702^{+0.104+0.232+0.393}_{-0.063-0.102-0.176}$	$0.708^{+0.014+0.111+0.159}_{-0.099-0.153-0.215}$	$0.733^{+0.037+0.185+0.321}_{-0.107-0.170-0.230}$
Ω_{k0}	N/A	$0.004^{+0.009+0.016+0.023}_{-0.004-0.010-0.015}$	N/A	$0.010^{+0.010+0.020+0.032}_{-0.004-0.014-0.018}$
$\sum m_\nu$ (eV)	N/A	N/A	$\sum m_\nu < 0.48$ (2σ)	$\sum m_\nu < 1.17$ (2σ)
H_0 (km/s/Mpc)	$70.3^{+1.3+2.9+4.2}_{-1.3-2.8-4.0}$	$70.7^{+1.7+3.1+4.6}_{-1.2-2.6-4.2}$	$69.6^{+1.8+3.3+4.8}_{-0.9-2.1-3.5}$	$71.0^{+1.1+2.8+4.2}_{-1.2-2.8-4.1}$
τ	$0.087^{+0.015+0.030+0.047}_{-0.013-0.026-0.038}$	$0.087^{+0.014+0.029+0.046}_{-0.015-0.026-0.037}$	$0.087^{+0.015+0.031+0.047}_{-0.011-0.023-0.036}$	$0.085^{+0.012+0.029+0.044}_{-0.009-0.024-0.035}$
Θ	$1.039^{+0.003+0.006+0.008}_{-0.002-0.004-0.006}$	$1.039^{+0.003+0.005+0.008}_{-0.001-0.004-0.006}$	$1.040^{+0.002+0.005+0.007}_{-0.003-0.005-0.007}$	$1.040^{+0.001+0.004+0.007}_{-0.002-0.005-0.008}$
n_s	$0.966^{+0.018+0.029+0.041}_{-0.010-0.020-0.031}$	$0.968^{+0.009+0.024+0.035}_{-0.015-0.025-0.037}$	$0.969^{+0.012+0.025+0.039}_{-0.011-0.023-0.032}$	$0.969^{+0.008+0.020+0.034}_{-0.016-0.032-0.046}$
$\log[10^{10}A_s]$	$3.181^{+0.036+0.070+0.107}_{-0.037-0.078-0.112}$	$3.188^{+0.039+0.081+0.120}_{-0.026-0.071-0.108}$	$3.172^{+0.039+0.072+0.115}_{-0.029-0.068-0.106}$	$3.191^{+0.039+0.097+0.123}_{-0.022-0.065-0.118}$
Ω_{de0}	$0.731^{+0.009+0.022+0.032}_{-0.015-0.029-0.043}$	$0.725^{+0.012+0.023+0.036}_{-0.018-0.036-0.053}$	$0.726^{+0.015+0.026+0.035}_{-0.012-0.025-0.038}$	$0.714^{+0.011+0.030+0.042}_{-0.023-0.048-0.073}$
Age (Gyr)	$13.875^{+0.076+0.183+0.284}_{-0.123-0.230-0.328}$	$13.708^{+0.115+0.410+0.671}_{-0.422-0.594-0.870}$	$13.869^{+0.093+0.241+0.378}_{-0.129-0.209-0.289}$	$13.480^{+0.244+0.566+0.819}_{-0.176-0.507-0.804}$
Ω_{m0}	$0.269^{+0.015+0.029+0.043}_{-0.009-0.022-0.032}$	$0.271^{+0.014+0.029+0.045}_{-0.009-0.023-0.032}$	$0.274^{+0.012+0.025+0.038}_{-0.015-0.026-0.035}$	$0.276^{+0.015+0.031+0.049}_{-0.010-0.023-0.033}$
z_{re}	$10.580^{+1.184+2.312+3.552}_{-1.106-2.251-3.447}$	$10.607^{+1.128+2.275+3.533}_{-1.187-2.317-3.472}$	$10.504^{+1.235+2.439+3.674}_{-0.908-2.075-3.210}$	$10.526^{+1.143+2.532+3.455}_{-0.703-2.083-3.213}$
CL for $c < 1$	4.2σ	2.5σ	4.6σ	2.7σ
$-\ln \mathcal{L}_{max} / \text{convergence}$	4009.2/0.0085	4008.9/0.0202	4009.2/0.0384	4008.7/0.0434

is some direct, non-gravitational interaction between holographic dark energy and dark matter, and such an interaction satisfies some conditions, the big rip can also be avoided [28, 52].

Figure 6 shows the results of the KHDE and VHDE models. In this figure, we only present the most interesting parameters for our discussions. It is seen that, compared with the HDE model, the KHDE model slightly favors a larger best-fit value of c . Moreover, the error bars of c are also enlarged. As shown in Fig. 5, for the HDE model, we have $c < 1$ at more than 4σ CL. However, as shown in the left panel of Fig. 6, after considering spatial curvature, we have $c < 1$ only in 2.5σ range.

This figure also shows the degeneracy situation of Ω_{k0} and c , in the KHDE model. It is clear that Ω_{k0} and c are in positive correlation. This result is well consistent with our previous work (see Fig. 4 of Ref. [52]; notice that the convention of Ω_{k0} in this paper is different from that in Ref. [52]). The best-fit value for Ω_{k0} is very close to zero, i.e., $\Omega_{k0} = 0.004$. The 2σ range of the spatial curvature is $-0.006 < \Omega_{k0} < 0.020$. Actually, the 3σ error bars of Ω_{k0} are still fairly small, also in order of 10^{-2} .

The constraints on the VHDE model are shown in the right panel of Fig. 6. One can see that, compared

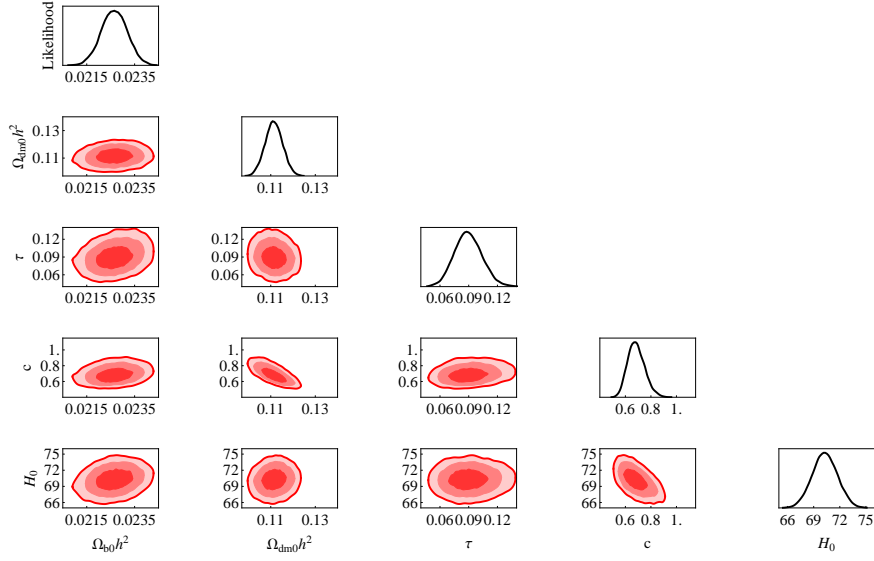


FIG. 5: The 1D marginalized distributions of individual parameters and 2D marginalized 1–3 σ CL contours, for the HDE model.

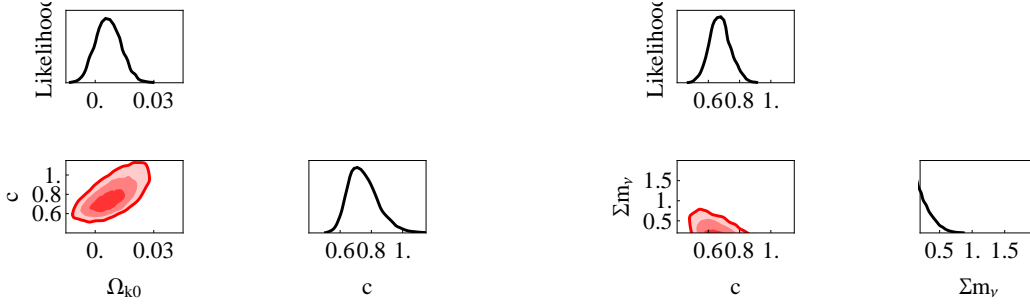


FIG. 6: The 1D marginalized distributions of individual parameters and 2D marginalized 1–3 σ CL contours, for the KHDE model (left panel) and the VHDE model (right panel). Here only the most relevant parameters are presented.

with the HDE model, the VHDE model also slightly favors a larger best-fit value of c . However, for the VHDE model, the changes on the error bars of c are quite different from the KHDE model: in the KHDE model, both the upper and the lower bounds of c are enlarged comparing to the HDE model; while in the VHDE model, although the lower bounds of c are enlarged, the upper bounds of c are reduced comparing to the HDE model. Moreover, for the VHDE model, we have $c < 1$ at 4.6 σ CL, which is quite similar to the result of the simplest HDE model. Therefore, we can conclude that the inclusion of massive neutrinos does not have significant influence on the phenomenological parameter c .

From the right panel of Fig. 6, one can also see that there is only weak negative correlation between

$\sum m_\nu$ and c , in the VHDE model. In addition, we obtain the upper bound of the total mass of neutrinos in the holographic dark energy model, $\sum m_\nu < 0.48$ eV at 2σ CL. This is the first result of the neutrino mass in the holographic dark energy model. For comparison, we mention here some results of neutrino mass in other dark energy scenarios. For a flat Λ CDM model, i.e., $w = -1$ and $\Omega_{k0} = 0$, Komatsu et al. [34] found that the WMAP+BAO+ H_0 limit is $\sum m_\nu < 0.58$ eV (95% CL). For a constant w model the results given by Komatsu et al. [34] are: $\sum m_\nu < 0.71$ eV (95% CL) from WMAP+LRG+ H_0 , and $\sum m_\nu < 0.91$ eV (95% CL) from WMAP+BAO+SN (where SN is the Constitution sample).

The results for the most sophisticated case, i.e. the KVHDE model, are shown in Fig. 7. We find that, for the KVHDE model, we have $c < 1$ only at the 2.7σ level.

This figure also shows the degeneracy situations of various parameters, in the KVHDE models. In the KHDE model we find that Ω_{k0} and c are in positive correlation, and in the VHDE model we do not observe significant correlation between $\sum m_\nu$ and c . So, we believe that the parameters Ω_{k0} and $\sum m_\nu$ should be in positive correlation. Indeed, in the KVHDE model, we find that the result is in accordance with the expectation. In addition, when simultaneously considering spatial curvature and massive neutrinos in the holographic dark energy model, the parameter space of $(\Omega_{k0}, \sum m_\nu)$ is greatly amplified. For example, the upper bound of $\sum m_\nu$ is enlarged by more than 2 times comparing to the VHDE model.

An interesting phenomenon in Table I is that the marginalized ranges of some cosmological parameters narrow when we add additional parameters. For example, compared with the HDE and KHDE models, the upper error bars of c shrink when we add $\sum m_\nu$ in the VHDE and KVHDE models. This phenomenon is understandable. In Fig. 7, we saw that a larger neutrino mass favors a smaller c , thus adding $\sum m_\nu$ into the fit will drag c to smaller values and shrink its upper error bars. Similar phenomenon also appears in other parameters. Due to the negative correlation with $\sum m_\nu$, we find narrow upper error bars of $100\Omega_{b0}h^2$ in the VHDE and KVHDE models, and the narrow upper error bars of n_s in KHDE and KVHDE models are due to its negative correlation with Ω_{k0} .³

In Fig. 8, we plot the CMB C_l^{TT} power spectra for the HDE, KHDE, VHDE and KVHDE models with the corresponding best-fit parameters. To make a comparison, we also include the Λ CDM model with the best-fit parameters given by the same set of data. It can be seen that the C_l^{TT} power spectra for the holographic dark energy are well inside the error bars of the observational data given by the WMAP 7-yr measurements and match the Λ CDM model very well.

Now, let us discuss the cosmological consequence of introducing spatial curvature and massive neutrinos in the holographic dark energy model. We are interested in the impacts of these factors on the EOS of dark

³ Since n_s is not our major focus, its contours are not plotted.

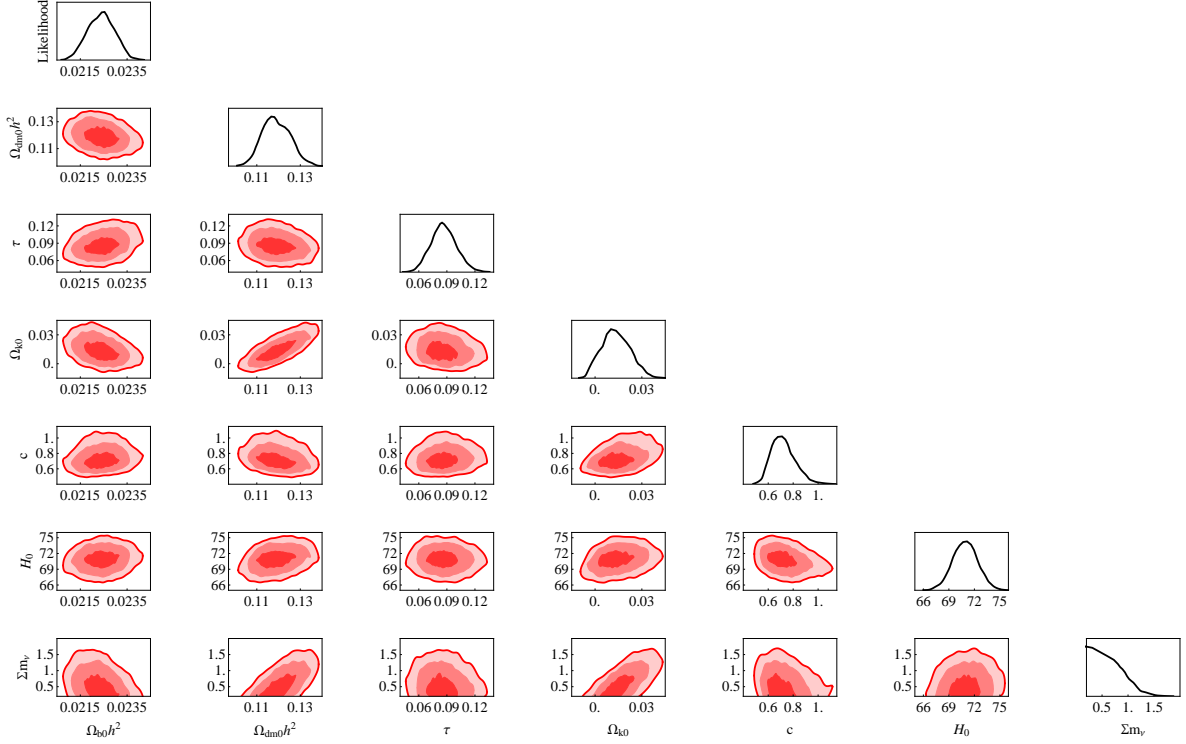


FIG. 7: The 1D marginalized distributions of individual parameters and 2D marginalized 1–3 σ CL contours, for the KVHDE model.

energy and the fate of the universe. Note that, if the spatial curvature is involved in the model, the EOS of the holographic dark energy reads

$$w = -\frac{1}{3} - \frac{2}{3} \sqrt{\frac{\Omega_{de}}{c^2} + \Omega_k}, \quad (22)$$

In the far future ($z \rightarrow -1$), it is clear that $\Omega_k \rightarrow 0$ and $\Omega_{de} \rightarrow 1$, and so we still have $w|_{z \rightarrow -1} = -\frac{1}{3} - \frac{2}{3c}$. Hence, even though the spatial curvature is involved, we still hold the conclusion that $c < 1$ leads to a Big Rip future singularity while for $c > 1$ this singularity is avoided.

In Fig. 9, we plot the evolution of w along with redshift z , including the best-fit results, as well as the 1–4 σ regions, for the considered models. As seen in the left panels of Fig. 9, for the holographic dark energy models without spatial curvature, w will cross -1 at more than 4 σ CL. As mentioned above, this means that the future universe will be dominated by phantom energy and will end up with a “Big Rip” singularity at more than 4 σ CL. As seen in the right panels of Fig. 9, after introducing the spatial curvature, w will cross -1 only in about 2.5 σ range. Therefore, the inclusion of spatial curvature in the holographic dark energy model may be helpful to alleviate the future cosmic doomsday problem. In contrast, the inclusion of massive neutrinos does not have significant influence on the evolution of $w(z)$.

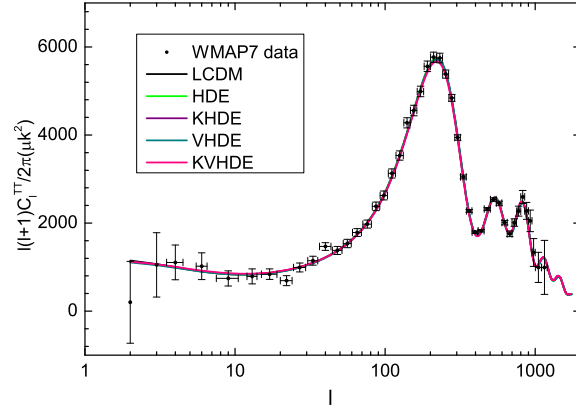


FIG. 8: The CMB C_l^{TT} power spectra for the HDE, KHDE, VHDE and KVHDE models with the corresponding best-fit parameter values. The black dots with error bars denote the observed data with their corresponding uncertainties from WMAP 7-yr results.

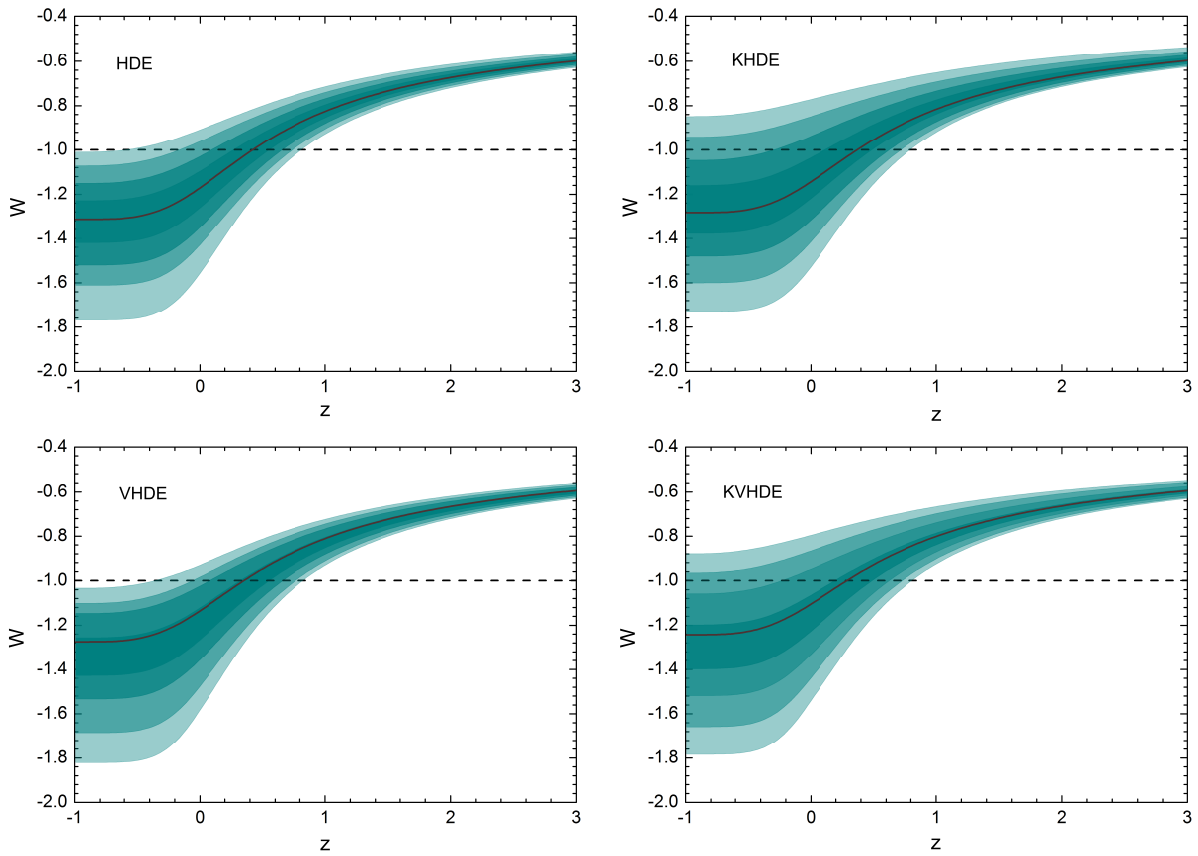


FIG. 9: The evolution of $w(z)$ along with redshift z , including the best-fit results, as well as the $1-4\sigma$ regions, for the considered models.

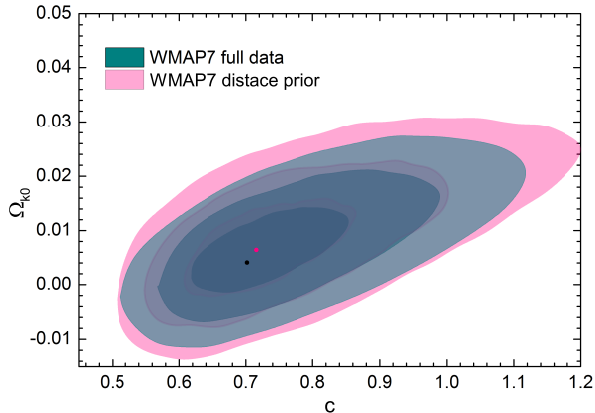


FIG. 10: The marginalized $1-3\sigma$ CL contours in the $c-\Omega_{k0}$ plane, for the KHDE model. The pink contours are plotted by using the WMAP distance priors, and the olive contours are plotted by using the full WMAP 7-yr data.

We also notice that the phantom behavior of the HDE model is different from many other models. The holographic dark energy is of phantom type at very high confidence levels. This is different from the 2- or 3- parametric scalar field dark energy models, Chaplygin gas models, divergence-free parametrization models, and so forth, where the phantom type of dark energy fits the same data only slightly better than the quintessence or cosmological constant models [34, 53–56]. This difference is due to the particular behavior of w in the HDE model. In the HDE model, there is always $w \rightarrow -\frac{1}{3}$ at high redshifts. However, from cosmological observations we know that on average there is $w \sim -1$. Thus, to fit the data, $w < -1$ is expected at low redshifts.

We are also interested in the differences between the cosmological constraints given by the WMAP 7-yr “distance priors” and those given by the full WMAP 7-yr data. As an example, we plot the marginalized $1-3\sigma$ CL contours in the $c-\Omega_{k0}$ plane, for the KHDE model, in Fig. 10. The pink contours are plotted by using the WMAP “distance priors”, and the olive contours are plotted by using the full WMAP data. As seen in this figure, the regions of the $1-3\sigma$ contours given by the full WMAP data are significantly smaller than the corresponding regions given by the WMAP “distance priors”. Therefore, making use of the full WMAP data can give better constraints on the holographic dark energy model, compared with the case using the WMAP “distance priors”.

IV. CONCLUDING REMARKS

In this paper we considered the holographic dark energy model with spatial curvature and massive neutrinos. It is well known that both the spatial curvature and neutrino mass are correlated with the dark energy EOS, so it is important to study the influences of these factors to the holographic dark energy. In addition,

it is also rather significant to consider the cosmological perturbations in holographic dark energy and make a global fit analysis on the holographic dark energy model.

We placed constraints on the holographic dark energy in a universe with spatial curvature and massive neutrinos, based on a MCMC global fit technique. The cosmic observational data include the WMAP 7-yr temperature and polarization data, the SNIa data from Union2.1 sample, the BAO data from SDSS DR7 and WiggleZ Dark Energy Survey, and the latest measurements of H_0 from HST. In order to treat the perturbations in dark energy when w crosses -1 , we employed the PPF approach. So, we do not suffer from the divergence problem when w crosses -1 .

We found that, for the simplest HDE model, the phenomenological parameter $c < 1$ at more than 4σ CL, showing that the future universe will be dominated by phantom dark energy at more than 4σ CL. After taking into account spatial curvature, we have $c < 1$ only in about 2.5σ range, implying that the inclusion of spatial curvature in the holographic dark energy model may be helpful to alleviate the future doomsday problem. In contrast, the inclusion of massive neutrinos does not have significant influence on the phenomenological parameter c .

For the KHDE model, we found that the 2σ range of the spatial curvature is $-0.006 < \Omega_{k0} < 0.020$; moreover, the 3σ error bars of Ω_{k0} are still fairly small, also in order of 10^{-2} . For the VHDE model, we obtained the result that the 2σ upper bound of the total mass of neutrinos is $\sum m_\nu < 0.48$ eV, which is the first result of neutrino mass in the holographic dark energy model. Moreover, when simultaneously considering spatial curvature and massive neutrinos, the upper bound of $\sum m_\nu$ will be enlarged by more than 2 times. Furthermore, we also demonstrated that, making use of the full WMAP 7-yr data can give better constraints on the holographic dark energy model, compared with the case using the WMAP ‘‘distance priors’’.

It should be mentioned that, there are still some factors not covered in our paper, e.g., the possible interaction between dark sectors. Evidently, when taking into account the interaction, the computation of the dark sector perturbations will become much more complicated. These issues deserve further investigations in the future work.

Acknowledgments

We would like to thank the anonymous referee for providing us with many helpful comments and suggestions, leading to significant improvement of this paper. This work was supported by the National Science Foundation of China under Grant Nos. 10705041, 10975032 and 11175042, and by the National Ministry

of Education of China under Grant Nos. NCET-09-0276 and N100505001.

-
- [1] A. G. Riess *et al.*, *AJ* **116**, 1009 (1998); S. Perlmutter *et al.*, *ApJ* **517**, 565 (1999).
- [2] D. N. Spergel *et al.*, *ApJS* **148**, 175 (2003); C. L. Bennet *et al.*, *ApJS* **148**, 1 (2003); D. N. Spergel *et al.*, *ApJS* **170**, 377 (2007); L. Page *et al.*, *ApJS* **170**, 335 (2007); G. Hinshaw *et al.*, *ApJS* **170**, 263 (2007).
- [3] M. Tegmark *et al.*, *Phys. Rev. D* **69**, 103501 (2004); *ApJ* **606**, 702 (2004); *Phys. Rev. D* **74**, 123507 (2006).
- [4] V. Sahni and A. Starobinsky, *Int. J. Mod. Phys. D* **9**, 373 (2000); P. J. E. Peebles and B. Ratra, *Rev. Mod. Phys.* **75**, 559 (2003); T. Padmanabhan, *Phys. Rept.* **380**, 235 (2003); E. J. Copeland, M. Sami and S. Tsujikawa, *Int. J. Mod. Phys. D* **15**, 1753 (2006); A. Albrecht *et al.*, astro-ph/0609591; J. Frieman, M. Turner and D. Huterer, *Ann. Rev. Astron. Astrophys* **46**, 385 (2008); S. Tsujikawa, arXiv:1004.1493; V. Sahni and A. Starobinsky, *Int. J. Mod. Phys. D* **15**, 2105 (2006); M. Li *et al.*, *Commun. Theor. Phys.* **56**, 525 (2011).
- [5] B. Ratra and P. J. E. Peebles, *Phys. Rev. D* **37**, 3406 (1988); P. J. E. Peebles and B. Ratra, *ApJ* **325**, L17 (1988); R. R. Caldwell, R. Dave and P. J. Steinhardt, *Phys. Rev. Lett.* **80**, 1582 (1998); I. Zlatev, L. Wang and P. J. Steinhardt, *Phys. Rev. Lett.* **82**, 896 (1999).
- [6] R. R. Caldwell, *Phys. Lett. B* **545**, 23 (2002); S. M. Carroll, M. Hoffman and M. Trodden, *Phys. Rev. D* **68**, 023509 (2003); R. R. Caldwell, M. Kamionkowski and N. N. Weinberg, *Phys. Rev. Lett.* **91**, 071301 (2003).
- [7] C. Armendariz-Picon, T. Damour and V. Mukhanov, *Phys. Lett. B* **458**, 209 (1999); C. Armendariz-Picon, V. Mukhanov and P. J. Steinhardt, *Phys. Rev. D* **63**, 103510 (2001); T. Chiba, T. Okabe and M. Yamaguchi, *Phys. Rev. D* **62**, 023511 (2000).
- [8] T. Padmanabhan, *Phys. Rev. D* **66**, 021301 (2002); J. S. Bagla, H. K. Jassal, and T. Padmanabhan, *Phys. Rev. D* **67**, 063504 (2003).
- [9] H. Wei, R. G. Cai, and D. F. Zeng, *Class. Quant. Grav.* **22**, 3189 (2005); H. Wei, and R. G. Cai, *Phys. Rev. D* **72**, 123507 (2005); H. Wei, N. N. Tang, and R. G. Cai, *Phys. Rev. D* **75**, 043009 (2007).
- [10] A. Y. Kamenshchik, U. Moschella and V. Pasquier, *Phys. Lett. B* **511**, 265 (2001); M. C. Bento, O. Bertolami and A. A. Sen, *Phys. Rev. D* **66**, 043507 (2002); X. Zhang, F. Q. Wu and J. Zhang, *JCAP* **0601**, 003 (2006).
- [11] W. Zhao and Y. Zhang, *Class. Quant. Grav.* **23**, 3405 (2006); T. Y. Xia and Y. Zhang, *Phys. Lett. B* **656**, 19 (2007); S. Wang, Y. Zhang and T. Y. Xia, *JCAP* **10** 037 (2008); S. Wang and Y. Zhang, *Phys. Lett. B* **669** 201 (2008).
- [12] M. Chevallier and D. Polarski, *Int. J. Mod. Phys. D* **10** 213 (2001); E. V. Linder, *Phys. Rev. Lett.* **90** 091301 (2003); D. Huterer and G. Starkman, *Phys. Rev. Lett.* **90** 031301 (2003); D. Huterer and A. Cooray, *Phys. Rev. D* **71** 023506 (2005); A. Shafieloo, V. Sahni and A. A. Starobinsky, *Phys. Rev. D* **80** 101301 (2009).
- [13] Q. G. Huang *et al.*, *Phys. Rev. D* **80** 083515 (2009); S. Wang, X. D. Li and M. Li, *Phys. Rev. D* **83** 023010 (2011); X. D. Li *et al.*, *JCAP* **07** (2011) 011; M. Li, X. D. Li and S. Wang, arXiv:0910.0717; S. Wang, X. D. Li and M. Li, *Phys. Rev. D* **82** 103006 (2010); X. D. Li, S. Wang, Q. G. Huang, X. Zhang and M. Li, *Sci. China Phys. Mech. Astron.* **55**, 1330 (2012); J. Z. Ma and X. Zhang, *Phys. Lett. B* **699**, 233 (2011); H. Li and

- X. Zhang, Phys. Lett. B **703**, 119 (2011); Y. H. Li and X. Zhang, Eur. Phys. J. C **71**, 1700 (2011).
- [14] G. 't Hooft, gr-qc/9310026; L. Susskind, J. Math. Phys. **36**, 6377 (1995).
- [15] A. G. Cohen, D. B. Kaplan and A. E. Nelson, Phys. Rev. Lett. **82**, 4971 (1999).
- [16] M. Li, Phys. Lett. B **603**, 1 (2004).
- [17] M. Li, C. S. Lin and Y. Wang, JCAP **0805**, 023 (2008).
- [18] X. Zhang and F. Q. Wu, Phys. Rev. D **76**, 023502 (2007); Z. Chang, F. Q. Wu and X. Zhang, Phys. Lett. B **633**, 14 (2006); J. Y. Shen, B. Wang, E. Abdalla and R. K. Su, Phys. Lett. B **609**, 200 (2005); Z. L. Yi and T. J. Zhang, Mod. Phys. Lett. A **22**, 41 (2007); M. Li, X. D. Li, S. Wang and X. Zhang, JCAP **0906**, 036 (2009); X. Zhang, Phys. Rev. D **79**, 103509 (2009); Z. P. Huang and Y. L. Wu, arXiv:1202.3517.
- [19] C. J. Hogan, astro-ph/0703775; arXiv:0706.1999; J. W. Lee, J. Lee and H. C. Kim, JCAP **0708**, 005 (2007); M. Li *et al.*, Commun. Theor. Phys. **51**, 181 (2009); M. Li and Y. Wang, Phys. Lett. B **687**, 243 (2010); M. Li, R. X. Miao and Y. Pang, Phys. Lett. B **689**, 55 (2010); M. Li, R. X. Miao and Y. Pang, Opt. Express **18**, 9026 (2010).
- [20] Q. G. Huang and Y. G. Gong, JCAP **0408**, 006 (2004); X. Zhang and F. Q. Wu, Phys. Rev. D **72**, 043524 (2005); B. Wang, E. Abdalla and R. K. Su, Phys. Lett. B **611**, 21 (2005); B. Wang, Y. G. Gong and E. Abdalla, Phys. Lett. B **624**, 141 (2005); B. Wang, C. Y. Lin and E. Abdalla, Phys. Lett. B **637**, 357 (2006). S. Nojiri and S. D. Odintsov, Gen. Rel. Grav. **38**, 1285 (2006); J. Zhang, X. Zhang and H. Y. Liu, Eur. Phys. J. C **52**, 693 (2007); C. J. Feng, Phys. Lett. B **633**, 367 (2008); H. Wei and R. G. Cai, Phys. Lett. B **655**, 1 (2007); R. G. Cai, Phys. Lett. B **657**, 228 (2007); C. Gao, F. Wu, X. Chen and Y. G. Shen, Phys. Rev. D **79**, 043511 (2009); Y. Z. Ma, Y. Gong and X. L. Chen, Eur. Phys. J. C **60**, 303 (2009). C. J. Feng and X. Zhang, Phys. Lett. B **680**, 399 (2009); J. F. Zhang *et al.*, Eur. Phys. J. C **72**, 2077 (2012).
- [21] Q. G. Huang and M. Li, JCAP **0408**, 013 (2004).
- [22] Q. G. Huang and M. Li, JCAP **0503**, 001 (2005); X. Zhang, Int. J. Mod. Phys. D **14**, 1597 (2005); Phys. Lett. B **648**, 1 (2007); Phys. Rev. D **74**, 103505 (2006); B. Chen, M. Li and Y. Wang, Nucl. Phys. B **774**, 256 (2007); J. F. Zhang, X. Zhang and H. Y. Liu, Phys. Lett. B **651**, 84 (2007); H. Wei and S. N. Zhang, Phys. Rev. D **76**, 063003 (2007); M. R. Setare, J. F. Zhang and X. Zhang, JCAP **0703**, 007 (2007); J. F. Zhang, X. Zhang and H. Y. Liu, Phys. Lett. B **659**, 26 (2008); Y. Z. Ma and X. Zhang, Phys. Lett. B **661**, 239 (2008); B. Nayak and L. P. Singh, Mod. Phys. Lett. A **24**, 1785 (2009); K. Y. Kim, H. W. Lee and Y. S. Myung, Mod. Phys. Lett. A **24**, 1267 (2009); Y. G. Gong and T. J. Li, Phys. Lett. B **683**, 241 (2010); Z. P. Huang and Y. L. Wu, arXiv:1202.4228.
- [23] X. Zhang, Phys. Lett. B **683**, 81 (2010).
- [24] H. C. Kao, W. L. Lee, F. L. Lin, Phys. Rev. D **71**, 123518 (2005).
- [25] Y. Gong, B. Wang, Y. Z. Zhang, Phys. Rev. D **72**, 043510 (2005).
- [26] M. Li, X. Li and X. Zhang, Sci. China Phys. Mech. Astron. **53**, 1631 (2010).
- [27] Z. Zhang *et al.*, Mod. Phys. Lett. A, **27**, 1250115 (2012).
- [28] Z. Zhang *et al.*, JCAP **06**, 009 (2012).
- [29] L. Xu, Phys. Rev. D **85**, 123505 (2012).
- [30] C. Clarkson, M. Cortes and B. A. Bassett, JCAP **0708**, 011 (2007).
- [31] H. Li and X. Zhang, Phys. Lett. B **713**, 160 (2012).

- [32] W. Fang, *et al.*, Phys. Rev. D **78** 103509 (2008); W. Fang, W. Hu, and A. Lewis, Phys. Rev. D **78** 087303 (2008).
- [33] E. Komatsu *et al.*, ApJS. **180**, 330 (2009).
- [34] E. Komatsu *et al.*, ApJS. **192**, 18 (2011).
- [35] C. P. Ma and E. Bertschinger, Astrophys. J. **455** 7 (1995).
- [36] G. B. Zhao, J. Q. Xia, M. Li, B. Feng and X. M. Zhang, Phys. Rev. D **72**, 123515 (2005).
- [37] W. Hu and I. Sawicki, Phys. Rev. D **76** 104043 (2007); W. Hu, Phys. Rev. D **77** 103524 (2008).
- [38] A. G. Sanchez, *et al.*, arXiv:1203.6616, MNRAS accepted.
- [39] S. DeDeo, R. R. Caldwell and P. J. Steinhardt, Phys. Rev. D **67**, 103509 (2003) [Erratum-ibid. D **69**, 129902 (2004)] [astro-ph/0301284].
- [40] R. Bean and O. Dore, Phys. Rev. D **69**, 083503 (2004) [astro-ph/0307100].
- [41] S. Hannestad, Phys. Rev. D **71**, 103519 (2005) [astro-ph/0504017].
- [42] J. -Q. Xia, Y. -F. Cai, T. -T. Qiu, G. -B. Zhao and X. Zhang, Int. J. Mod. Phys. D **17**, 1229 (2008) [astro-ph/0703202].
- [43] R. de Putter, D. Huterer and E. V. Linder, Phys. Rev. D **81**, 103513 (2010) [arXiv:1002.1311 [astro-ph.CO]].
- [44] G. Ballesteros and J. Lesgourgues, JCAP **1010**, 014 (2010) [arXiv:1004.5509 [astro-ph.CO]].
- [45] R. U. H. Ansari and S. Unnikrishnan, arXiv:1104.4609 [astro-ph.CO].
- [46] A. Lewis and S. Bridle, Phys. Rev. D **66**, 103511 (2002).
- [47] <http://lambda.gsfc.nasa.gov/>.
- [48] N. Suzuki *et al.*, arXiv:1105.3470.
- [49] W. J. Percival *et al.*, MNRAS **401**, 2148 (2010).
- [50] M. Drinkwater *et al.*, MNRAS **401**, 1429 (2010); C. Blake *et al.*, arXiv:1108.2635, MNRAS accepted.
- [51] A. G. Riess *et al.*, Astrophys. J. **730**, 119 (2011).
- [52] M. Li *et al.*, JCAP **12**, 014 (2009).
- [53] P. -Y. Wang, C. -W. Chen and P. Chen, arXiv:1208.6579 [astro-ph.CO].
- [54] B. Novosyadlyj, O. Sergijenko, R. Durrer and V. Pelykh, Phys. Rev. D **86**, 083008 (2012) [arXiv:1206.5194 [astro-ph.CO]].
- [55] K. Liao, Y. Pan and Z. -H. Zhu, arXiv:1210.5021 [astro-ph.CO].
- [56] X. -D. Li, S. Wang, Q. -G. Huang, X. Zhang and M. Li, Sci. China G **55**, 1330 (2012) [arXiv:1202.4060 [astro-ph.CO]].